This is a repository copy of *New approach for modelling strain induced precipitation of Nb(C,N) in HSLA steels during multipass hot deformation in austenite*.

White Rose Research Online URL for this paper:
http://eprints.whiterose.ac.uk/9784/

Article:
Nagarajan, V., Palmiere, E.J. and Sellars, C.M. (2009) New approach for modelling strain induced precipitation of Nb(C,N) in HSLA steels during multipass hot deformation in austenite. Materials Science and Technology, 25 (9). pp. 1168-1174. ISSN 0267-0836

https://doi.org/10.1179/174328409X455242

Reuse
Unless indicated otherwise, fulltext items are protected by copyright with all rights reserved. The copyright exception in section 29 of the Copyright, Designs and Patents Act 1988 allows the making of a single copy solely for the purpose of non-commercial research or private study within the limits of fair dealing. The publisher or other rights-holder may allow further reproduction and re-use of this version - refer to the White Rose Research Online record for this item. Where records identify the publisher as the copyright holder, users can verify any specific terms of use on the publisher's website.

Takedown
If you consider content in White Rose Research Online to be in breach of UK law, please notify us by emailing eprints@whiterose.ac.uk including the URL of the record and the reason for the withdrawal request.

eprints@whiterose.ac.uk
https://eprints.whiterose.ac.uk/

New approach for modelling strain induced precipitation of Nb(C,N) in HSLA steels during multipass hot deformation in austenite

V. Nagarajan, E. J. Palmiere* and C. M. Sellars

A new model for strain induced precipitation of Nb(C,N) is developed from the existing model for single pass hot deformation. This new model can be extended to multipass deformation to explain the microstructural evolution during the hot deformation of Nb supersaturated high strength low alloy (HSLA) steels. The key feature of this model is the microband geometry employed, which leads to determination of the local solute concentration at microbands, and hence the potential for carbonitride precipitation on the microbands. The model also validates the need for concurrent growth and coarsening processes, even at the early stages of precipitation. The evolution of the precipitate radius, number density and volume fraction are compared with the experimental results obtained from thin foil TEM micrographs on Fe–30 wt-%Ni alloys (that are austenitic at room temperature and are similar to HSLA steels in deformation behaviour) subjected to deformation by plane strain compression. The model predictions are in good agreement with experimental results.

Keywords: Strain induced precipitation, Modelling, Model austenite, Hot deformation, HSLA steels

Published by Maney Publishing (c) IOM Communications Ltd

Introduction

Control of process parameters in steel industries has direct implications for the quality of the steels produced. A perfect understanding of the metallurgical phenomena occurring in the production process is very much required in order to control it. Internal microstructure plays a significant role in determining mechanical properties of steels and so, it is essential to have the right microstructure in the steel to obtain a good combination of mechanical properties. It is hence required to uncover the mechanism/kinetics of microstructural changes that take place within the steel during its processing, in order to have a good control over the process. In microalloyed steels, the strain induced precipitation (SIP) of the microalloying elements during thermomechanical processing plays an important role in controlling the final microstructure of the steel. Evolution of these precipitates during the industrial hot rolling process holds the key in understanding and controlling the process. The SIP of Nb(C,N) during the finishing temperatures associated with controlled rolling of Nb high strength low alloy (HSLA) steels plays an important role in stopping austenite recrystallisation, and thereby accumulating the strains over several rolling passes, which in turn enhances the sites for the nucleation of low temperature transformation products during cooling. The mechanism of strain induced precipitation has been studied greatly by several researchers.[1–11] A detailed illustration of mechanism and kinetics of strain induced precipitation was first given by Dutta *et al.*[4] and a mathematical model based on thermodynamics and experimental observation was later proposed by Dutta *et al.*[12] Several researchers[13–15] have used the Dutta model for the modelling of SIP of Nb(C,N) in HSLA steels. However, most of these models were proposed for single pass deformation and very little has been done on the modelling of multipass deformation in microalloyed steels. Sellars and Palmiere[16] have formulated the initial concepts for the modelling of precipitation kinetics for SIP for multipass hot deformation in microalloyed steels. The present paper aims to use these concepts and develop a new mathematical model for SIP of Nb(C,N) in microalloyed steels that could be easily extended to multipass deformation process.

Institute of Microstructural and Mechanical Processing Engineering, The University of Sheffield, Mappin Street, Sheffield S1 3JD, UK

*Corresponding author, email e.j.palmiere@sheffield.ac.uk

Experimental procedure

Alloy selection

The alloy composition chosen is given in Table 1. The steel contained 30 wt-%Ni in order to fully stabilise the austenite down to room temperature, which in turn would aid in the direct observation of precipitates and its location on dislocation structure by electron microscopy, without any interference from stray dislocations that would otherwise form during austenite to ferrite or martensite transformations as in C–Mn microalloyed steels.[17] The steel was vacuum melted at Corus Swinden Technology Centre (Rotherham), with a base

© 2009 Institute of Materials, Minerals and Mining
Published by Maney on behalf of the Institute
Received 1 May 2008; accepted 29 April 2009
DOI 10.1179/174328409X455242

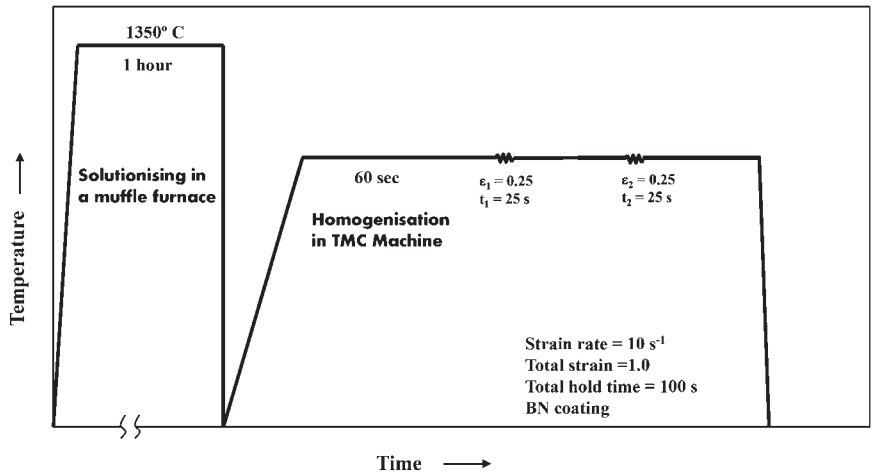

1 Schematic illustration of thermomechanical test cycle used to simulate industrial hot plate rolling with two deformation passes

composition of 1·5Mn–0·01P–0·006S–0·4Si–0·004N (wt-%) and hot rolled into strips of width 150 mm and thickness 15 mm. It is worth noting that the base composition is typical of commercially produced C–Mn steels. However, the compositions shown in Table 1, particularly the Nb concentration, are not typical of industrial microalloyed steel grades, which often have Nb and C present in ratios of 0·2–0·5. For analytical purposes, this research wanted to maximise the extent of Nb(C,N) precipitation, thus selecting Nb and C concentrations such that the Nb/C ratio was near stoichiometry. Furthermore, as the increased Ni concentration decreases the solubility of Nb(C,N) in austenite by a factor of ~2·5 at the temperatures of interest, a higher addition of Nb is required in this model alloy than what would be necessary in a conventional C–Mn microalloyed steel to create similar supersaturations.[17,18]

Plane strain compression (PSC) tests

The as rolled strips were solutionised in a muffle furnace at 1350°C for 1·5 h, to dissolve all of the microalloying elements,[19] quenched in iced water and machined to standard dimensions ($60 \times 30 \times 10$ mm) for PSC testing.[20] The specimens were then loaded into the thermomechanical compression test machine and rapidly heated (at a rate of ~20°C s^{-1}) to 1200°C to redissolve all the carbides that may have reprecipitated while quenching after the solutionising treatment. Specimens were held at 1200°C to allow for equilibrium and were then cooled at a rate of 50°C s^{-1} to the respective deformation temperature. Under isothermal conditions, a two pass thermomechanical processing cycle (Fig. 1) was used in order to determine the incremental hardening between the deformation processes due to strain induced precipitation. The conditions of strain, strain rate and deformation temperature used are typical of those used for the industrial rolling of microalloyed plate steel. A total strain of 1·0 and strain rate of 10 s^{-1} was maintained for all tests with varying interpass times for different tests. The test temperatures ranged from 800 to 1000°C.

Electron microscopy

Thin foils were prepared from the PSC test samples using standard procedures and were analysed to determine both the precipitate size and distribution on a Philips 420 TEM. A thin sheet of specimen was first ground mechanically on both sides until 1200 grit emery paper, to a thickness of ~70 μm and then 3 mm discs were punched out from this foil. The discs were then subjected to twin jet electropolishing using an electrolyte of 5% perchloric acid, 35% butoxy ethanol and 60% methanol.

Model

Microband geometry

The key feature of this new model is its ability to be extended to a multipass deformation scheme. The original Dutta[4] model considered the bulk solute concentrations in computing the precipitate size evolutions. In this new model, local solute concentrations are considered. In order to perform this, it is required to have a specific geometry for the microband. It is well known that deformation microstructure in austenite shows roughly parallel bands of slightly differing lattice orientations.[17] The misorientation across the microband is accommodated by a dense network of dislocations called microbands. A simplified geometry for such a microband is shown in Fig. 2.[16] As illustrated in Fig. 2, the dislocation networks in the x–y planes represent the geometrically necessary dislocations required to accommodate the misorientation across each microband for two adjacent microbands. For typical misorientations, the spacing of these dislocations h, is 10 to 50 nm and the spacing of the microbands w, in the z direction is 500 to 2000 nm.[21] Therefore, in Fig. 2 the scale used on the x and y axes is 2·5 times larger than that used on the z axis. If all the dislocation nodes are potential sites for

Table 1 Chemical composition of alloy along with Nb(C,N) dissolution temperature and Nb/C ratio

Alloy	C, wt-%	Nb, wt-%	NbC dissolution temperature, °C	Nb/C ratio
Fe–30 wt-%Ni	0·05	0·38	1189	7·6

Published by Maney Publishing (c) IOM Communications Ltd

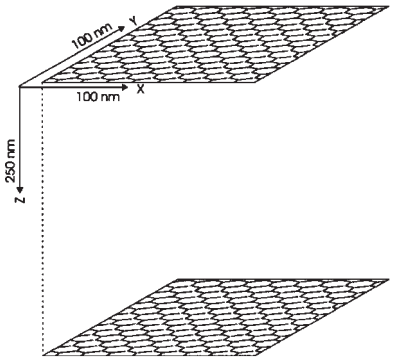

2 Schematic diagram of geometry of dislocation microband structure after one deformation pass assumed in model

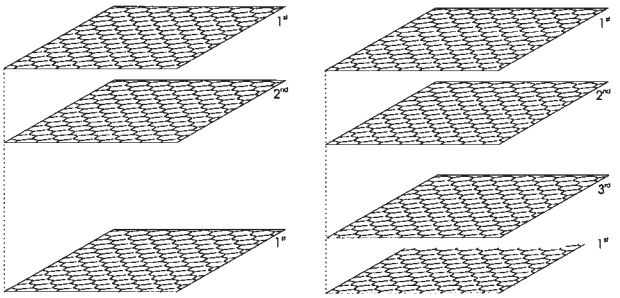

3 Schematic diagram of geometry of dislocation structure *a* after second pass following precipitation on dislocation nodes on first generation and *b* after third pass following precipitation on dislocation nodes in second generation microbands

the nucleation of carbide particles, it can be seen that precipitates will be close together in the x–y plane, so that particle coarsening by diffusion in this plane will start at relatively short times compared with those for complete precipitation, which requires diffusion of niobium from the matrix over the much longer distances in the z direction. This feature of the geometry thus leads directly to consistency with the experimental observation[17,18,22] and the conclusion of the earlier model[12] that the number density of precipitates decreases with time from a maximum value at an early stage of the precipitation process. The geometry also allows simple separation of the growth of precipitates by bulk diffusion in the z direction and the coarsening by bulk and/or pipe diffusion in the x–y plane. This greatly facilitates extension of the model to multipass deformation. The model assumes that all the dislocation nodes act as potential sites for carbonitride precipitation. The density of nodes for the above mentioned geometry is given by equation (1)

$$N_o = \frac{2{\cdot}3}{h^2 w} \tag{1}$$

The spacing h, between the dislocations in the microband depends on the mean misorientation angle across the microband which increases with the applied strain ε, as $\theta = a\varepsilon$, where a is a constant. Assuming that the microbands are formed only by a series of edge dislocations would give $\theta = \mathbf{b}/h$, where $\mathbf{b}$ is the Burgers vector and using a value[17] for the mean misorientation of 2° would lead to

$$h = 7{\cdot}4 \times 10^{-9} \varepsilon^{-1} \tag{2}$$

The spacing w, between the microbands is given by

$$w = \frac{16}{\rho^{1/2}} \tag{3}$$

The dislocation density ρ, depends on the extent of work hardening in the alloy and is given by

$$\rho = \left(\frac{\sigma - \sigma_y}{M \alpha G \mathbf{b}}\right)^2 \tag{4}$$

where σ and σ_y are the flow and yield stresses of the material, M is the Taylor factor (=3·1) α is a constant (≈0·15) and G is the shear modulus.

When strain induced precipitates are formed, the overall pinning force offered by the precipitates on the microband would depend on the size of the precipitates. For the times of interest in industrial hot rolling operations (plate), it is reasonable to assume that the precipitates sizes are very fine (few nanometres) and such fine precipitates offer very high pinning forces thereby increasing the Orowan stresses dramatically making the microband rigid. Any further deformation is to be accommodated by the formation of new microbands, as shown in Fig. 3.

The effectiveness of the newly formed microbands, to provide potential sites for precipitate nucleation depends on the level of supersaturation of solute element at the vicinity of the new microband. A niobium concentration profile between the microbands, at the end of interpass time after first deformation, is clearly required to determine the efficacy/potential of nucleation of precipitates on the next generation of microbands. The concentration profile between the microbands is obtained by solving the diffusion equation in two dimensions, using finite difference scheme,[23] and where D represents the bulk diffusivity of Nb in Fe.

$$\frac{\partial C}{\partial t} = D\left(\frac{\partial^2 C}{\partial x^2} + \frac{\partial^2 C}{\partial y^2}\right) \tag{5}$$

The solute concentration at the microband is taken as the boundary condition for solving this diffusion equation. The interdislocation spacing is so small that the diffusion takes place almost instantly between them and hence the solute concentration at the microband is assumed to be same as the solute concentration at the precipitate/matrix interface C_r, given by the Gibbs–Thomson equation

$$C_r = C_{Nb}^{eq} \exp\left(\frac{2\gamma V_m}{R_p R_g T}\right) \tag{6}$$

where γ (= 0·5 J m^{-2}) is the interfacial energy between the precipitate matrix interface, R_g is the universal gas constant, T is the absolute temperature, V_m is the molar volume of precipitate, R_p is the precipitate radius and C_{Nb}^{eq} is the equilibrium solute concentration and is given by[24]

$$C_{Nb}^{eq} = \frac{10^{2{\cdot}06 - 6700/T}}{C_C + (12/14)C_N} \tag{7}$$

Model description

Thermal activation of atoms in the material causes concentration fluctuations forming clusters of solute

Published by Maney Publishing (c) IOM Communications Ltd

atoms. When a solute cluster of a size greater than a critical radius is reached, a stable nucleus is formed. This critical radius is derived from thermodynamic considerations of the driving force for the formation of precipitates[12]

$$R_c = \frac{-2\gamma}{\Delta G_v} \tag{8}$$

$$\Delta G_v = -\frac{R_g T}{V_m} \ln (k_s) \tag{9}$$

$$k_s = \frac{C_{Nb}\left[C_C + (12/14)C_N\right]}{10^{2\cdot06 - 6770/T}} \tag{10}$$

where C_{Nb}, C_C and C_N are the concentrations of Nb, C and N respectively in the alloy. For stability of the precipitate formed, it is assumed that the first formed precipitate is 5% greater than the critical radius, thus

$$R_p = 1\cdot05 R_c \tag{11}$$

The rate at which the precipitate radius grows by diffusion during the growth stage is given by the following equation[6]

$$\frac{dR_p}{dt} = \frac{D}{R_p}\frac{\left(C_{Nb} - C_{Nb}^{eq}\exp\left(R_o/R_p\right)\right)}{\left(C_{Nb}^{ppt} - C_{Nb}^{eq}\exp\left(R_o/R_p\right)\right)} + \frac{1}{N}\frac{dN}{dt}\left(\eta R_c - R_p\right) \tag{12}$$

where C_{Nb}^{ppt} is Nb concentration in the precipitate, N is the precipitate number density, η is a factor representing the size of the newly formed precipitate as compared to the critical radius R_c for nucleation and $R_o = 2\gamma V_m/R_g T$

The diffusion distances between the precipitates are very small because the interdislocation spacing h, is very small (measured to be 10–50 nm), and hence equilibrium is reached very quickly between the precipitates and the matrix within a narrow band of region at the microband. Thus as the precipitates are growing by diffusion of solute atoms to the microband region from the matrix region between the microbands, coarsening starts to take place on the microband through capillarity action between the precipitates on the microband in this narrow band of region at the microband. Hence, growth and coarsening takes place concurrently. The rate at which the precipitates coarsen is given by[10,25,26]

$$\left.\frac{dR_p}{dt}\right|_{coarsening} = \frac{4}{27}\left(\frac{C_{Nb}^{eq}}{C_{Nb}^{p} - C_{Nb}^{eq}}\right)\left(\frac{R_o D}{R_p^2}\right) \tag{13}$$

Results

Plane strain compression test

The high temperature flow curves from the PSC tests are shown in Fig. 4. All of the curves presented in Fig. 4 have been corrected both for the effects of friction as well as any rise in temperature due to deformational heating. It is clear from Fig. 4 that strain induced precipitation occurred at all four deformation temperatures (800, 850, 900 and 1000°C), which is evident from the increase in the flow stress between the first and the second deformation pass. This incremental increase in strength is tabulated in Table 2 which shows a general trend of increasing strength with increasing deformation temperature and then decreasing again, which is when precipitate coarsening becomes a dominant process.

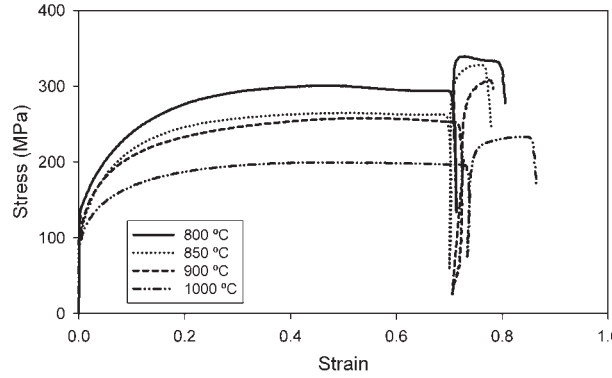

4 Isothermal stress–strain curves for different deformation temperatures obtained from PSC tests conducted on thermomechanical compression machine

Electron microscopy

The TEM micrographs of thin foils from two as deformed PSC specimens tested at 850°C with an interpass delay time of 25 and 50 s is shown in Fig. 5. The orientations of all micrographs are such that the compression axis runs horizontal to the page. In all but Fig. 5*d*, it is clear that the precipitates are present in a linear arrangement and lie on the microband, which is typical of strain induced precipitation. There are two kinds of precipitates in these micrographs:

(i) the precipitates that formed in the undeformed sample before deformation started (large precipitates lying randomly in the matrix, clearly illustrated by Fig. 5*e* and *f*, and removed from the analysis of the SIPs)

(ii) precipitates formed by strain induced precipitation (fine particles lying on the microbands, Fig. 5*a–c*, *e* and *f*).

The average precipitate diameters measured for the two test samples were $11\cdot6 \pm 0\cdot2$ nm and $13\cdot0 \pm 0\cdot6$ nm for 25 and 50 s interpass delay times respectively (based on the examination of $\sim$10 foils for each deformation condition). The distribution of precipitate diameters following quantitative analysis are shown in Fig. 6.

Model

A precipitate of radius R_p is first formed and with this as the boundary condition for the diffusion equation, a

Table 2 Incremental hardening obtained from stress–strain curves tested at different deformation temperatures

Temperature, °C	Hold time, s	Total strain	Incremental hardening, MPa
800	$1+Q$	0·75+0·25	39
850	25+25	0·75+0·25	64
900	25+25	0·75+0·25	58
1000	25+25	0·75+0·25	34

Published by Maney Publishing (c) IOM Communications Ltd

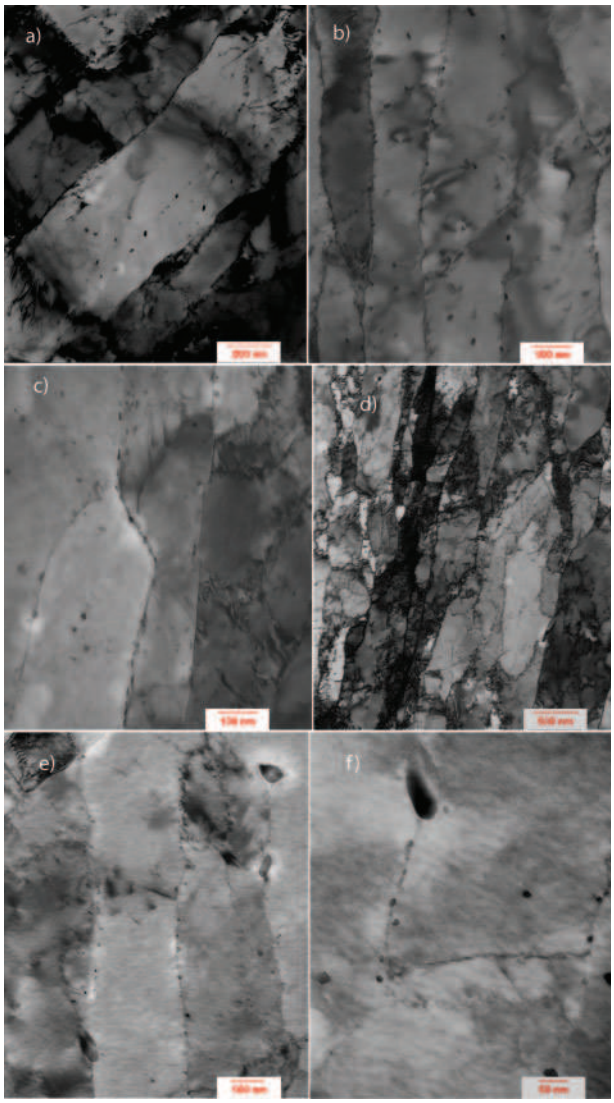

a–c micrographs of sample deformed to strain of 0·75, held for 25 s and again deformed to strain of 0·25 and quenched; *d–f* micrographs of sample deformed to strain of 0·75 held for 25 s and again deformed to strain of 0·25, held for 25 s and quenched (total 50 s holding time)

5 Images (TEM) of samples tested at 850°C for two pass deformation scheme: large precipitates (such as those illustrated in top right of *e* and top centre left of *f*) are those which have either been undissolved or those which have precipitated before deformation commenced; compression axis runs horizontally across page

new concentration profile between the microbands is computed. The flux of atoms, involved in the formation of these precipitates can be calculated from the new concentration profile. From the calculated flux, the precipitation fraction X can be computed. This precipitation fraction when multiplied by the equilibrium precipitate volume fraction V_o, gives the actual precipitate volume fraction XV_o. If the precipitate number density is represented by N, then using a mass balance

$$N = \frac{XV_o}{(4/3)\pi R_p^3} \tag{14}$$

Therefore, the precipitate volume fraction is calculated for every iteration from the solute concentration profile

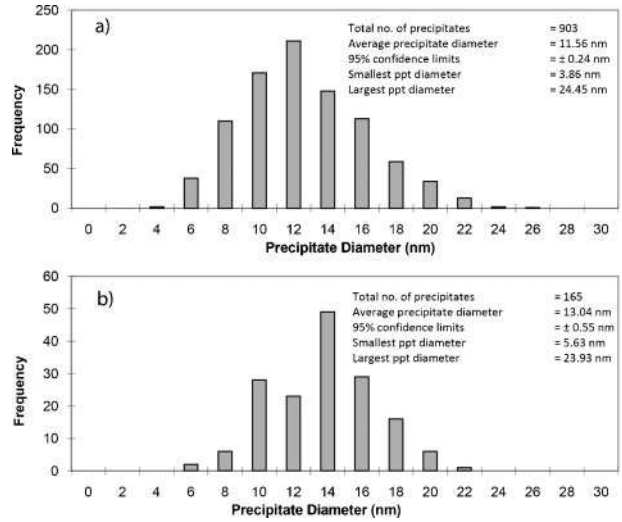

a sample deformed to strain of 0·75, held for 25 s and again deformed to strain of 0·25 and quenched; *b* sample deformed to strain of 0·75 held for 25 s and again deformed to strain of 0·25, held for 25 s and quenched

6 Precipitate size distribution obtained from TEM micrographs (Fig. 5) of samples tested at 850°C for two pass deformation scheme

and the precipitate number density is computed accordingly (equation (14)) to comply with the precipitate growth rate equation. The results from this computer model simulating a 50 s hold at 850°C after a deformation to a strain level of 1·0 are shown in Fig. 7. Figure 7*a* gives the solute concentration profile between microbands (a two-dimensional network of microbands is considered) at the end of 50 s. The precipitate number density and precipitate radius evolution are shown in Fig. 7*b* and *c* respectively. Figure 7*d* and *e* gives the precipitate volume fraction and fraction of equilibrium precipitation (precipitation fraction) while Fig. 7*f* gives the solute concentration on the microband.

Discussion

Plane strain compression tests

The flow curves presented in Fig. 4 show significant incremental strengthening occurring during the interpass times between deformation passes. Furthermore, as shown in Table 2, an incremental strengthening of 39 MPa even for an exceptionally short interpass time of 1 s at a deformation temperature of 800°C indicates that the precipitation kinetics in this model alloy are very fast. This is more clearly shown in the precipitation–time–temperature diagram (Fig. 8) which shows two C curves for precipitation in undeformed austenite; homogeneous precipitation occurring within the grain interior and heterogeneous precipitation occurring on the grain boundaries. Superimposing the temperature profile of the test specimen (obtained from the PSC test) onto the C curves gives us an understanding on the speed of the precipitation kinetics. First, the time to precipitation on grain boundaries is ~5 orders of magnitude shorter than that for homogeneous precipitation. The nose of this curve lies at ~45 s for 900°C. The superimposed temperature profile cuts the C curve even before the deformation starts. Therefore, partial precipitation of Nb(C,N) would take place in the

Published by Maney Publishing (c) IOM Communications Ltd

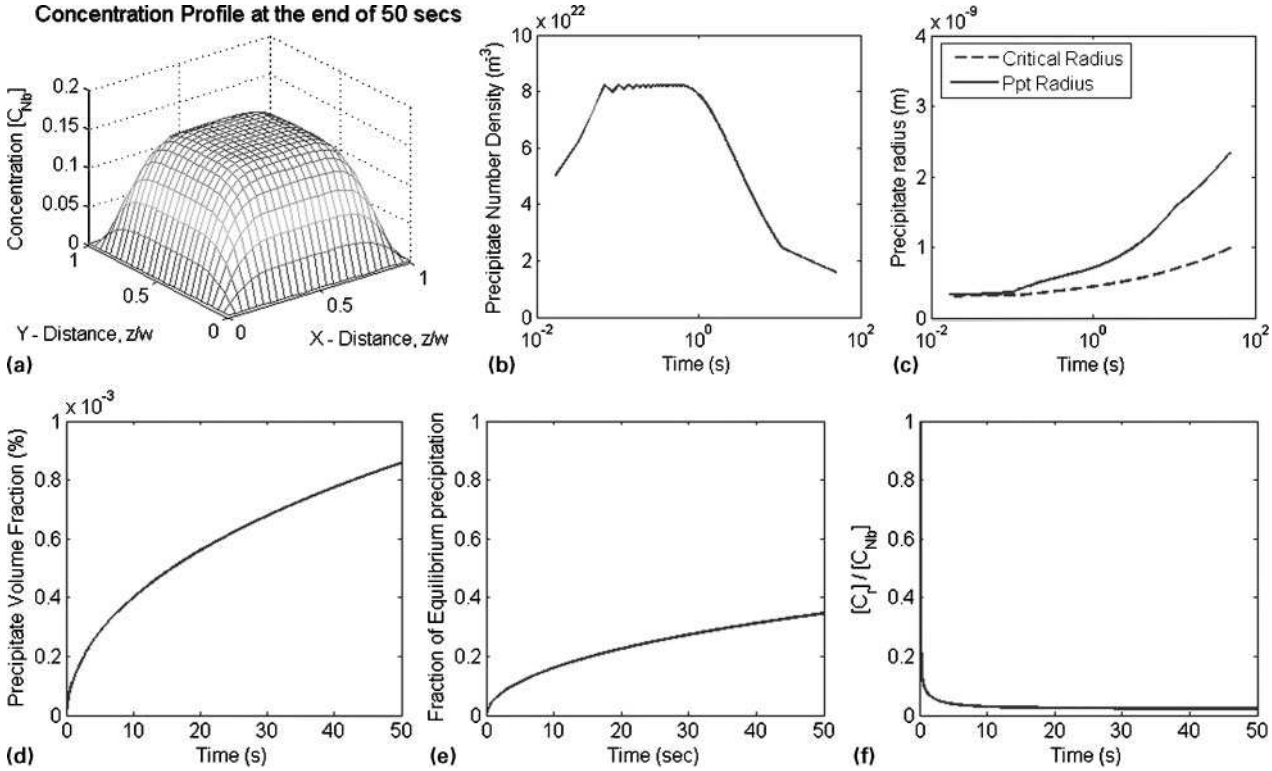

a solute concentration profile between two-dimensional network of microbands (as function of *z* normalised by microband spacing *w*); *b* precipitate number density; *c* precipitate radius evolution; *d* precipitate volume fraction; *e* fraction of equilibrium precipitation (precipitation fraction); *f* solute concentration on microband sample

7 Illustration of results from computer model: deformation to equivalent strain of 1 and held for 50 s at 850°C

undeformed austenite on the grain boundaries. These predeformation precipitates would reduce the total niobium supersaturation in the alloy, thereby reducing the precipitation potential for strain induced precipitation.

Electron microscopy

The fast precipitation kinetics for this alloy speaks for the presence of large precipitates in the TEM micrographs shown in Fig. 5. It is believed that these large precipitates are those that were formed even before deformation has commenced. In order to confirm this, a sample that was interrupted from thermomechanical processing cycle and quenched just before the deformation was investigated. The TEM micrographs of this sample contained large precipitates of Nb(C,N) along with very few small precipitates. This is shown in Fig. 9*b* alongside Fig. 9*a*, which shows no precipitation following the solution heat treatment of 1350°C followed by quenching.

The shape of the precipitate size distribution histogram shown in Fig. 6 is typical of a microstructure that has coarsened. Such a shape is seen in both the samples with 25 and 50 s of interpass hold times, which is a clear indication that coarsening has started well before 25 s and further confirms the assumption used in the model that coarsening of precipitates starts at a very early stage in the precipitation process.

Model

The model prediction for precipitate radius at the end of 50 s of hold at 850°C after a deformation strain of 1·0 is

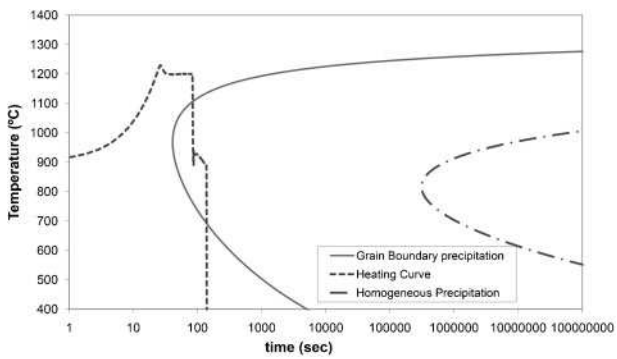

8 Precipitation–time–temperature diagram for alloy showing start time for grain boundary precipitation: heating profile that sample underwent during test is superimposed on this which is shown by thick broken lines

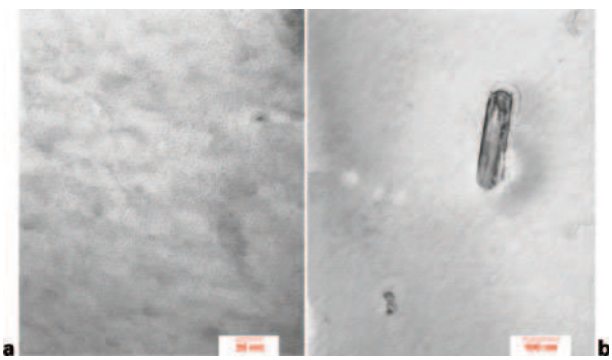

9 Images (TEM) of *a* solutionised sample showing no precipitates at all (complete solutionisation) and *b* sample that underwent heating part of thermomechanical process and quenched just before start of deformation

Published by Maney Publishing (c) IOM Communications Ltd

2·4 nm (diameter 4·8 nm). The actual precipitate diameter measured on the TEM micrographs for the PSC test sample that went through the same test conditions is 13·0 nm (Fig. 6). The actual measured diameter is slightly greater than the predicted diameter by a factor of ~ 2. Two main reasons could be attributed to this discrepancy. First, the smallest precipitate diameter that was detected on the TEM micrographs was 3·9 nm. It is difficult to distinguish other image contrasts on the micrographs from the precipitates at these small sizes. If one were able to detect/measure all the finer precipitates, the average measured precipitate size would tend to decrease from what is measured now. Second, the model uses r^3 law for coarsening (assuming bulk diffusion). Considering the grain boundary diffusion (r^4 law)[25,27] or the pipe diffusion (r^5 law)[25–27] would enhance the coarsening rate and hence would increase the predicted precipitate radius somewhat. Thus these two effects would narrow down the gap between the predicted and the measured values for precipitate radius. Considering this fact, we could say that the model prediction is reasonably in good agreement with the experimentally measured value.

The original Dutta[4] model used the bulk solute concentration values and hence the whole model could not be extended to multipass. The new approach in modelling strain induced precipitation proposed here has the advantage of knowing the local solute concentration at the microband and in the region between the microbands. With the knowledge of the precipitate radius it is possible to calculate the pinning forces offered by the precipitates on the microband and hence one can find out if the second deformation would be accommodated by the already available microband or by the formation of a new generation of microbands. The precipitation potential of this next generation of microbands purely depends on the local solute concentration. This will form the basis of future work.

Conclusion

Images of TEM confirm the occurrence of strain induced precipitation. However, its full effect was not seen, owing to the partial reprecipitation of niobium even before the deformation commenced. The numerical model prediction agrees reasonably well with the experimental observation. The model further supports the theory that growth and coarsening of precipitates takes place concurrently during the strain induced precipitation process. This new model will form the base for a multipass model.

Acknowledgement

The authors express their sincere thanks to Niobium Products Company, Germany for sponsoring this research and Corus RD&T (Swinden Technology Centre) for providing laboratory casts together with Professor A.A. Howe for his useful discussions.

References

1. R. Abad, A. I. Fernandez, B. Lopez and J. M. Rodriguez-Ibabe: *ISIJ Int.*, 2001, **41**, 1373–1382.
2. M. G. Akben, I. Weiss and J. J. Jonas: *Acta Metall.*, 1981, **29**, 111–121.
3. B. Dutta and C. M. Sellars: 'Strengthening of austenite by Nb(C,N) precipitation in niobium HSLA steels', Proc. Int. Conf. on 'Physical metallurgy of thermomechanical processing of steels and other metals', Tokyo, Japan, June 1988, Iron and Steel Institute of Japan, 261–268.
4. B. Dutta, E. Valdes and C. M. Sellars: *Acta Mater.*, 1992, **40**, 653–662.
5. S. S. Hansen, J. B. Vander-Sande and M. Cohen: *Metall. Trans. A*, 1980, **11A**, 387–402.
6. K. Kliber and I. Schindler: *J. Mater. Process. Technol.*, 1996, **60**, 597–602.
7. O. Kwon and A. J. DeArdo: *Acta Metall. Mater.*, 1991, **39**, 529–538.
8. S. F. Medina and A. Quispe: *ISIJ Int.*, 1996, **36**, 1295–1300.
9. E. V. Pereloma, B. R. Crawford and P. D. Hodgson: *Mater. Sci. Eng. A*, 2001, **299**, 27–37.
10. B. Dutta and E. J. Palmiere: *Metall. Mater. Trans. A*, 2003, **34A**, 1237.
11. R. M. Poths, W. M. Rainforth and E. J. Palmiere: *Mater. Sci. Forum*, 2005, **500–501**, 139–146.
12. B. Dutta, E. J. Palmiere and C. M. Sellars: *Acta Mater.*, 2001, **49**, 785–794.
13. N. Fujita and H. K. D. H. Bhadeshia: *Mater. Sci. Technol.*, 2001, **17**, 403.
14. H. S. Zurob, Y. Brechet and G. Purdy: *Acta Mater.*, 2001, **49**, 4183–4190.
15. H.S. Zurob, C. R. Hutchinson, Y. Brechet and G. Purdy: *Acta Mater.*, 2002, **50**, 3075–3092.
16. C. M. Sellars and E. J. Palmiere: *Mater. Sci. Forum*, 2005, **500–501**, 3–14.
17. W. M. Rainforth, M. P. Black, R. L. Higginson, E. J. Palmiere, C. M. Sellars, I. Prabst, P. Warbichler and F. Hofer: *Acta Mater.*, 2002, **50**, 735–747.
18. M. P. Black: 'Microstructural Evolution of Austenite in a Microalloyed Fe-30 wt% Ni Alloy', PhD thesis, The University of Sheffield, Sheffield, UK, 2002, 159.
19. R. M. Poths, R. L. Higginson and E. J. Palmiere: *Scr. Mater.*, 2001, **44**, 147–151.
20. M. S. Loveday, G. J. Mahon, B. Roebuck, A. J. Lacey, E. J. Palmiere, C. M. Sellars and M. R. van der Winden: *Mater. High Temp.*, **23**, 2006, 85–118.
21. C. M. Sellars and B. P. Wynne: Proc. 25th Riso Int. Symp. on 'Materials science. evolution of deformation microstructures in 3D', (ed. C. Grundlach *et al.*), 117–126; 2004, Roskilde, Riso National Laboratory.
22. B. Dutta and C. M. Sellars: *Mater. Sci. Technol.*, **3**, 1987, 197–207.
23. M. Dehgan: *Appl. Math. Comput.*, 2003, **138**, 489–501.
24. E. J. Palmiere, C. I. Garcia and A. J. DeArdo: *Metall. Mater. Trans. A*, 1994, **25A**, 277–286.
25. A. J. Ardell: *Acta Metall.*, 1972, **20**, 601–609.
26. K. Miyata, T. Omura, T. Kushida and Y. Komizo: *Metall. Mater. Trans. A*, 2003, **34A**, 1565–1573.
27. M. V. Speight: *Acta Metall.*, 1968, **16**, 133–135.

Published by Maney Publishing (c) IOM Communications Ltd